



# Synthesis and characterization of 9,10-substituted anthracene derivatives as blue light-emitting and hole-transporting materials for electroluminescent devices

A-monrat Thangthong, Duangratchaneekorn Meunmart, Narid Prachumrak, Siriporn Jungstittiwong, Tinnagon Keawin, Taweesak Sudyoadsuk, Vinich Promarak\*

Center for Organic Electronic and Alternative Energy, Department of Chemistry and Center for Innovation in Chemistry, Faculty of Science, Ubon Ratchathani University, Warinchumrap, Ubon Ratchathani 34190, Thailand

## ARTICLE INFO

### Article history:

Received 20 October 2011  
Received in revised form 21 December 2011  
Accepted 29 December 2011  
Available online 3 January 2012

### Keywords:

Anthracene  
Blue light-emitting material  
Hole-transporting material  
Triphenylamine  
Organic light-emitting diode

## ABSTRACT

New 9,10-substituted anthracene derivatives were designed and synthesized for application as blue-emitting and hole-transporting materials in electroluminescent devices. They were characterized by H NMR, C NMR, FTIR, UV–vis, PL spectroscopy, and mass spectrometry. The theoretical calculation of three-dimensional structure and the energy densities of HOMO and LUMO states, as well as optical properties of these new obtained materials, supported the claim that they had non-coplanar structures. Their optical, thermal, and electrochemical properties could be tuned by varying the peripheral substituents. All of them were electrochemically and thermally stable molecules. Materials having electron donating triphenylamine as peripheral substituents showed promising potential as both blue light-emitting materials and hole-transporting materials for electroluminescent devices. Efficient blue and Alq3-based green OLEDs with maximum luminance efficiencies and CIE coordinates of 1.65 cd/A and (0.15, 0.16) and 6.25 cd/A and (0.26, 0.49) were achieved, respectively.

© 2012 Elsevier Ltd. All rights reserved.

## 1. Introduction

The use of  $\pi$ -conjugated organic compounds as electroluminescent materials in organic light-emitting diodes (OLEDs) was originally introduced by van Slyke over two decades ago.<sup>1</sup> Since then, the development of new  $\pi$ -conjugated compounds especially small molecules with superior physical, optical, thermal, and electrochemical properties has become one of the most reviving research areas.<sup>2–4</sup> OLEDs for flat-panel displays are showing great promise, and a related application for a flexible flat-panel display is progressing.<sup>5</sup> Full-color displays are required for red, green, and blue light-emitting materials. Although many fluorescent blue emitters have been reported, such as anthracene derivatives,<sup>6</sup> phenylene derivatives,<sup>7</sup> pyrene derivatives,<sup>8</sup> fluorene derivatives,<sup>9</sup> carbazole derivatives,<sup>10</sup> triarylamine derivatives,<sup>11</sup> and phosphorescent iridium complexes,<sup>12</sup> there is still a clear need for further improvements in terms of efficiency and color purity compared to red and green emitters.

Due to its unique chemical and electron-rich structure, low electronic band gap and strong blue fluorescence, anthracene

has received considerable interest. Anthracene derivatives have been extensively used as fluorescent chromophores in the construction of chemosensors for many applications.<sup>13</sup> Incorporation of anthracene and its 9,10-substituted derivatives into polymer main-chains<sup>14</sup> or linked as pendent groups<sup>15</sup> contributes to solve the problem of preparation of films with good optical quality or to suppress excimer formation. A number of polymeric and molecular 9,10-substituted anthracenes have also been developed and studied as blue light-emitting materials for OLED devices.<sup>6,15,16</sup> However, new classes of anthracene based-blue light-emitters with improvements in terms of efficiency and color purity remain to be explored. In this work, the designed 9,10-substituted anthracenes incorporating different characteristic aromatic rings such as fluorene, thiophene, and triphenylamine as  $\pi$ -conjugation substituents were synthesized and characterized (Fig. 1). The introduction of planar thiophene would allow a long  $\pi$ -conjugation system to be achieved, while integration of the bulky triphenylamine could suppress aggregation of the planar anthracene ring, as well as increase the hole-transporting capability and thermal stability.<sup>17</sup> Fluorene also has a number of advantages, including its capability to emit in the blue part of the visible spectrum, chemical and photochemical stability.<sup>9,18</sup> The physical and photophysical properties of these compounds were investigated with the aim of

\* Corresponding author. Tel.: +6 645 353 401x4510; fax: +6 645 288 379; e-mail addresses: [pvinich@ubu.ac.th](mailto:pvinich@ubu.ac.th), [pvinich@gmail.com](mailto:pvinich@gmail.com) (V. Promarak).

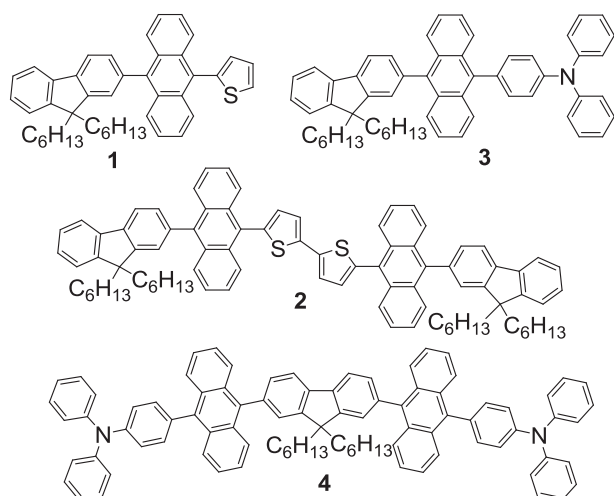


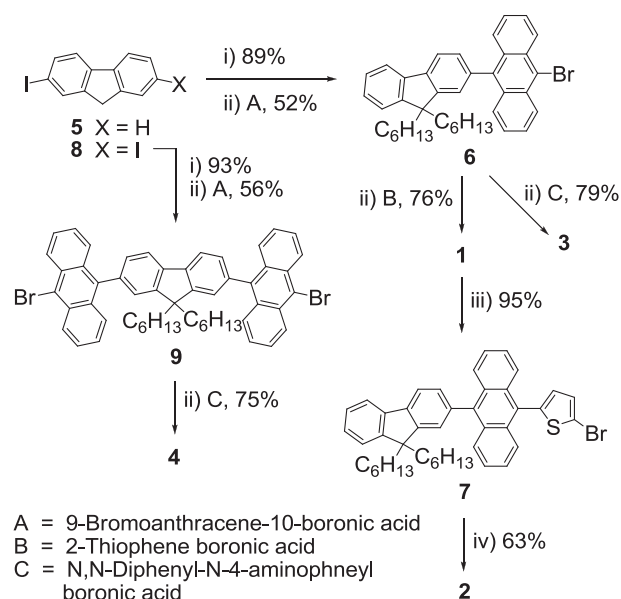
Fig. 1. Chemical structures of 9,10-substituted anthracenes 1–4.

understanding the structure–property relationships and developing novel molecular  $\pi$ -conjugated materials. Investigations on OLED device fabrication and characterization are also demonstrated.

## 2. Results and discussion

### 2.1. Synthesis

The molecular structures of the target anthracenes bearing fluorene, thiophene, bithiophene, and triphenylamine as 9,10-substituents are shown in Fig. 1. As illustrated in Scheme 1, we began the synthesis with alkylation of 2-iodofluorene **5**<sup>19</sup> at C-9 position of the fluorene ring with dihexyl chains followed by palladium-catalyzed Suzuki cross-coupling of the resultant in excess amounts with 9-bromoanthracene-10-boronic acid to give **6** in a fair yield of 52%. Target anthracene **1** bearing fluorene and thiophene rings as 9,10-substituents was formed by Suzuki cross-coupling of **6** with 2-thiopheneboronic acid in 76% yield as light yellow solids. To form the more extended  $\pi$ -conjugation molecule of **2**, a two-step synthesis was carried out by regioselective bromination at  $\alpha$ -position of thiophene ring of **1** with NBS in THF followed by reductive nickel-catalyzed dimerization reaction of the obtained **7** with the catalytic system of NiCl<sub>2</sub>, zinc powder, PPh<sub>3</sub>, and bipyridine (bpy) in DMAc at 90 °C. Anthracene **2**, a dimer of **1**, was obtained as a greenish solid in an overall yield of 60%. In the target anthracenes **3** and **4**, a substituent group with a hole-transporting property was introduced. Compound **3** bearing fluorene and triphenylamine as substituents was obtained as a light yellow solid in a good yield of 79% by Suzuki cross-coupling of readily formed **6** with *N,N*-diphenyl-*N*-4-aminophenylboronic acid.<sup>20</sup> Target anthracene **4**, a dimer of **3**, was successfully synthesized by carrying out double Suzuki cross-coupling of ready dialkylated 2,7-diiodofluorene **8**<sup>19</sup> with 9-bromoanthracene-10-boronic acid (2.11 equiv) followed by coupling of the obtained **9** with *N,N*-diphenyl-*N*-4-aminophenylboronic acid, and gained as a deep yellow solid in 75% yield. All newly synthesized compounds were fully characterized by standard spectroscopic methods. They had good solubility in most organic solvents at room temperature, resulting from the presence of *n*-hexyl groups at the C-9 of fluorene ring. As a result, no crystallization thin film should be obtained from a solution casting.



Scheme 1. Synthetic route to 1–4. Reagents and conditions: (i) 50% NaOH, *n*-Bu<sub>4</sub>NBr, C<sub>6</sub>H<sub>13</sub>Br, DMSO, rt; (ii) Pd(PPh<sub>3</sub>)<sub>4</sub>, 2 M Na<sub>2</sub>CO<sub>3</sub>, THF, reflux; (iii) NBS, THF, rt; (iv) NiCl<sub>2</sub>, Zn, PPh<sub>3</sub>, DMAc, bpy, 90 °C.

### 2.2. Quantum calculation and optical properties

To understand the electronic properties and the geometries of 1–4, quantum chemical calculations were performed using the TDDFT/B3LYP/6-31G (d,p) method.<sup>21</sup> The optimized structures of these compounds revealed that all molecules adopted non-co-planar conformations. Particularly, the planar anthracene unit was twisted nearly perpendicular to the adjacent thiophene, fluorene, and triphenylamine moieties because of a steric repulsion between anthracene *peri*-hydrogen atoms (1,8 and 4,5 positions) and hydrogen atoms of those aromatic rings. Such structural characteristics can influence some of their electronic and physical properties such as a suppression of the conjugation. As demonstrated in Fig. 2

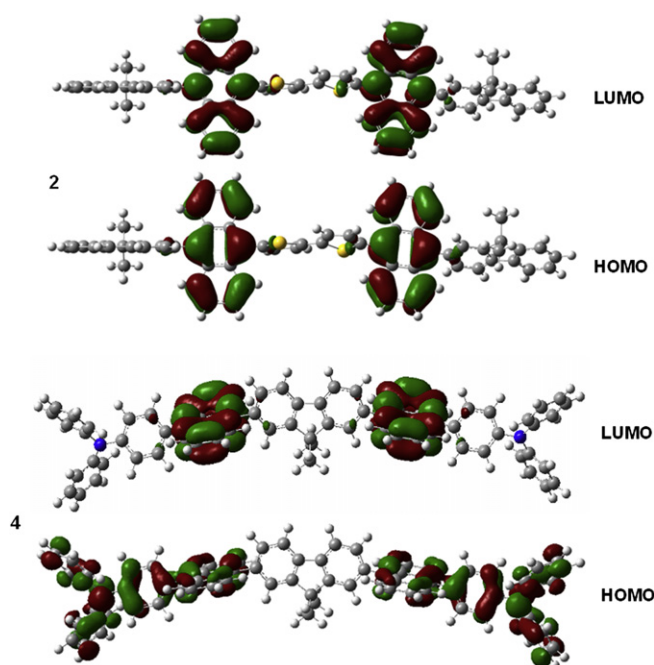


Fig. 2. The HOMO (bottom) and LUMO (top) orbitals of 2 and 4.

(also see Supplementary data), in the highest occupied molecular orbitals (HOMO) of **1** and **2**,  $\pi$ -electrons are located on the anthracene and thiophene moieties, while in the HOMO orbitals of **3** and **4**,  $\pi$ -electrons are delocalized over anthracene and donor triphenylamine segments. The participation of the fluorene ring in the  $\pi$ -conjugation system was diminished in all cases. In the lowest unoccupied molecular orbitals (LUMO) of all compounds, electrons located only on anthracene rings. The HOMO–LUMO energy gaps ( $E_g$  calcd) were calculated and presented in Table 1. These calculated values slightly deviated from those obtained from the experimental results ( $\sim 0.01$ – $0.18$  eV). There are factors responsible for the errors because the orbital energy difference between HOMO and LUMO is still an approximate estimation of the transition energy, since the transition energy also contains significant contributions from some two-electron integrals. The real situation is that an accurate description of the lowest singlet excited state requires a linear combination of a number of excited configurations.

**Table 1**  
Physical and photophysical data of **1**–**4**

Compd	$\lambda_{\text{abs}}^a$ (nm)	$\lambda_{\text{em}}^a$ (nm)	$\lambda_{\text{em}}^b$ (nm)	Stokes shift <sup>c</sup> (nm)	$\Phi_F^d$	$T_g/T_c/T_m/T_{5d}^e$ (°C)	$E_g^f$ (eV)	$E_g$ calcd <sup>g</sup> (eV)	$E_{1/2}^h$ (V)	$E_{\text{onset}}^h$ (V)	HOMO/LUMO <sup>i</sup> (eV)
<b>1</b>	359, 378, 398	439	439	41	0.12	—/115/209/330	2.96	3.11	1.20, 1.45	1.12	–5.56/–2.60
<b>2</b>	363, 383, 402	474	483	72	0.04	—/—/326/370	2.87	3.05	1.15, 1.40	1.08	–5.52/–2.65
<b>3</b>	359, 380, 399	484	458	85	0.73	79/—/—/397	2.90	2.93	0.95, 1.21	0.88	–5.32/–2.42
<b>4</b>	360, 380, 400	485	466	85	0.77	155/225/338/424	2.89	2.90	0.96, 1.25	0.88	–5.32/–2.43

<sup>a</sup> Measured in a dilute  $\text{CH}_2\text{Cl}_2$  solution.

<sup>b</sup> Measured on a vapor deposition thin film and excited at 390 nm.

<sup>c</sup> Stokes shift calculated from the difference between  $\lambda_{\text{max}}$  of the absorption and emission spectra.

<sup>d</sup> Determined in  $\text{CH}_2\text{Cl}_2$  solutions ( $A < 0.1$ ) at room temperature using quinine sulfate solution in 0.01 M  $\text{H}_2\text{SO}_4$  ( $\Phi_F = 0.54$ ) as a standard.<sup>23</sup>

<sup>e</sup> Obtained from DSC on the second heating cycle and TGA measurements under  $\text{N}_2$  at a heating rate of  $10^\circ\text{C}/\text{min}$ .

<sup>f</sup> Estimated from the onset of the absorption spectra ( $E_g = 1240/\lambda_{\text{onset}}$ ).

<sup>g</sup> Obtained from quantum chemical calculation using TDDFT/ B3LYP/6-31G (d,p).

<sup>h</sup> Measured using a three-electrode system fitted with a glassy carbon working electrode, a platinum rod counter electrode, and SCE reference electrode in degassed  $\text{CH}_2\text{Cl}_2$  containing 0.1 M  $n\text{-Bu}_4\text{NPF}_6$  as a supporting electrolyte at a scan rate of 50 mV/s.

<sup>i</sup> Calculated using the empirical equation:  $\text{HOMO} = -(4.44 + E_{\text{onset}})$  and  $\text{LUMO} = \text{HOMO} + E_g$ .

Photophysical properties of **1**–**4** were investigated in dilute  $\text{CH}_2\text{Cl}_2$  solution and thin film obtained by thermal evaporation on quartz substrate. The pertinent data are presented Figs. 3 and 4, and summarized in Table 1. Their UV–vis spectra showed two absorption bands, which were assigned in terms of the strong absorption band in the region of 250–310 nm corresponding to the  $\pi$ – $\pi^*$  local electron transition of the individual aromatic units, and the less intense three absorption bands in the region of 350–400 nm attributed to the characteristic  $\pi$ – $\pi^*$  electron transition of the anthracene. Their HOMO–LUMO energy gaps ( $E_g$ ) were estimated from the onset of the absorption spectra to be 2.96, 2.87, 2.90, and 2.89 eV, respectively. The  $E_g$ s of **3** and its corresponding dimer **4**

were nearly identical, despite somewhat different molecular sizes, indicating they had comparable  $\pi$ -conjugation length. This can be explained by an out of plane twisting of the fluorene unit from adjacent anthracene rings as mentioned earlier (Fig. 2) limiting the delocalization of  $\pi$ -electrons on the anthracene and triphenylamine units only. In contrast, the  $E_g$  of **1** is noticeably higher than that of its corresponding dimer **2** indicating remarkably longer  $\pi$ -conjugation length in **2**. This is due to less a hindered thiophene ring in the molecules allowing extended  $\pi$ -electron delocalization over the anthracene and bithiophene moieties.

These compounds in solution fluoresced ranging from bright blue to blue-green colors with featureless photoluminescence (PL) spectra (Fig. 3), which is similar to what was observed for most 9,10-diphenylanthracenes.<sup>6</sup> The solution PL spectrum of the dimer **2** red-shifted with respect to that of **1**, whereas the PL spectra of **3** and dimer **4** were duplicate. These results were in agreement to what was observed from the theoretical and UV–vis experiments. These

materials showed a slight Stokes shift (41–85 nm) suggesting less energy loss during the relaxation process and efficient fluorescence. The thin film PL emission spectrum of **1**, shown in Fig. 4, was similar to its solution PL spectrum in terms of line shape, emission  $\lambda_{\text{max}}$  and full width at a half-maximum, thus indicating or less, if any, solid state packing occurred in this case due to its bulky molecular structure. However, the thin film PL spectrum of **2** exhibited a bathochromic shift caused by solid state packing, thus indicating greater planarity between the anthracene and bithiophene units

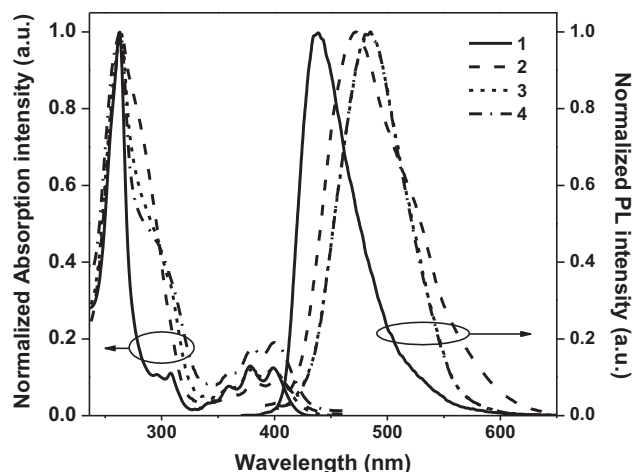


**Fig. 3.** UV–vis absorption and PL spectra of **1**–**4** measured in dilute  $\text{CH}_2\text{Cl}_2$  solution.

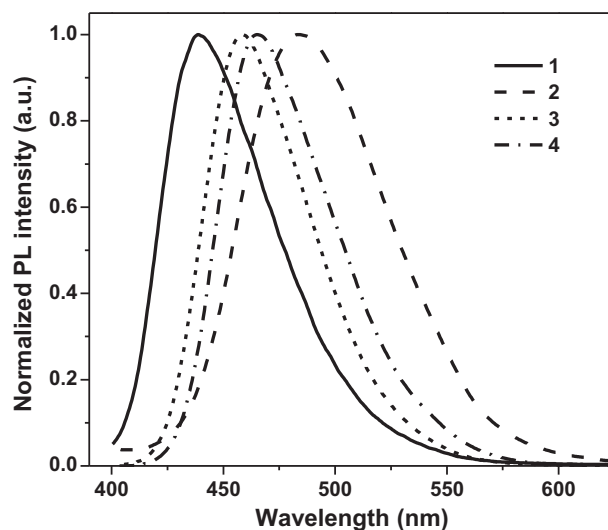


**Fig. 4.** PL spectra of **1**–**4** measured as thin film obtained by vapor deposition on quartz substrate.

and better  $\pi$ -electron delocalization in the conjugated system. In the cases of **3** and **4** having bulky structures, their thin film PL spectra exhibited a hypsochromic shift of about 19–26 nm compared to their corresponding solution spectra. This result may also be attributed to the aforementioned solid state packing force, which prohibits the electron-vibration coupling between the triphenylamine substituent and the anthracene photoactive unit.

Fluorescence quantum yields ( $\Phi_F$ ) of **1–4** measured in dilute solution using quinine sulfate solution in 0.01 M  $H_2SO_4$  ( $\Phi_F=0.54$ ) as a standard were 0.12, 0.04, 0.73 and 0.77, respectively. The results indicated that direct attachment of the thiophene ring to the luminous anthracene moiety in compound **1** lowered the  $\Phi_F$  (0.12) and the value was rather reduced in compound **2** ( $\Phi_F=0.04$ ) having two thiophene rings. The decrease in  $\Phi_F$  value with the increase in the thiophene units is usually observed in most of the thiophene oligomers as the molecule becoming more planar and likely to fluorescence quenching by intermolecular  $\pi$ - $\pi$  stacking.<sup>22</sup> In contrast, replacing the thiophene ring with electron donating triphenylamine in compound **3** significantly increased the  $\Phi_F$  (0.73) and the value was slightly higher in the dimer **4** ( $\Phi_F=0.77$ ).

### 2.3. Electrochemical and thermal properties

Electrochemical behaviors of all compounds were investigated by cyclic voltammetry (CV) and the resulting data are shown in Fig. 5 and summarized in Table 1. The experiment was carried out in degassed  $CH_2Cl_2$  containing 0.1 M  $n-Bu_4NPF_6$  as a supporting electrolyte under argon atmosphere. Compound **3** and its corresponding dimer **4** were found to exhibit two quasi-reversible oxidation processes at 0.95 and 1.21 V, and 0.96 and 1.26 V, respectively. The first oxidation wave was assigned to the removal of electrons from the peripheral triphenylamines resulting in radical cations, while the second was attributed to the formation of an anthracene radical cation. The onset oxidation potentials ( $E_{onset}$ ) of **3** and **4** estimated from the first anodic oxidation wave were at the same value of 0.88 V, which is very close to the data reported for most triphenylamine derivatives (0.90 V). Their multiple CV scans revealed identical CV curves with no additional peak at a lower potential on the cathodic scan ( $E_{pc}$ ) being observed (see Supplementary data). This indicates that no oxidative coupling, or a weak oxidative coupling if any at the *p*-phenyl rings of the peripheral triphenylamine, led to electro-polymerization and electrochemically stable molecules. Usually, this type of electrochemical coupling reaction is detected in most triphenylamine derivatives with an unsubstituted at *p*-position of the phenyl ring as in case of 2,7-bis[2-(4-

diphenylaminophenyl)-1,3,4-oxadiazol-5-yl]-9,9-bis-*n*-hexylfluorene.<sup>24</sup> Steric hindrance of an adjacent anthracene ring might play a key role in preventing such electrochemical reactions in both molecules. CV curves of **1** and **2** showed two irreversible oxidation processes. Duplicate CV curves of each compound were noticed under multiple scans demonstrating stable molecules (see Supplementary data). In the case of **1**, the first oxidation wave corresponds to the removal of electrons from the terminal thiophene ring to form the radical cation. No oxidation peak at a lower potential due to a dimerization coupling of such species was detected, unlike what was observed in most cases of  $\alpha$ -unsubstituted short oligothiophenes.<sup>25</sup> In our case, this electrochemical dimerization coupling could be prevented by a steric hindrance of the nearby anthracene moiety. Moreover, under these CV experiment conditions, no distinct reduction process was observed in all cases. The HOMO and LUMO energy levels of **1–4** were calculated from the oxidation onset potentials ( $E_{onset}$ ) and energy gaps ( $E_g$ ) and the results are summarized in Table 1. The HOMO levels of these materials ranged from  $-5.56$  to  $-5.32$  eV matching well with the work functions of the gold (Au) or indium tin oxide (ITO) electrodes and favoring the injection and transport of holes.

The thermal properties of **1–4** were investigated by the thermogravimetric analysis (TGA) and differential scanning calorimetry (DSC), and the results are shown in Fig. 5 and summarized in Table 1. These results suggest that all compounds were thermally stable materials with 5% weight loss temperatures ( $T_{5d}$ ) well over 330 °C. During the first heating DSC scan of crystalline samples **1** and **2**, only endothermic melting peaks ( $T_m$ ) at 209 and 328 °C were detected, respectively. In their DSC second heating scan, the thermogram of **1** showed broad exothermic peaks due to the crystallization ( $T_c$ ) at 115 °C followed by the melting peak, while the second heating thermogram of dimer **2** was the same as the first cycle. Compounds **3** and **4** bearing triphenylamine as a substituent exhibited different thermal behavior. The asymmetric nature of this group may play an additional role to the molecular packing. The DSC thermogram (first scan) of **3** only revealed an endothermic peak at 155 °C due to melting of the crystalline sample, while under a second heating cycle, only endothermic baseline shift owing to glass transition ( $T_g$ ) at 79 °C was detected with no crystallization and melting peaks at higher temperature being observed. The thermogram (second scan) of **4** displays  $T_g$  at 155 °C and  $T_c$  around 225 °C to give the same crystals as obtained by crystallization from solution, which then melted at 338 °C. The ability of **3** and **4** to form a molecular glass with the possibility to prepare thin films from these materials both by evaporation and by solution casting is highly desirable for applications in electroluminescent devices (Fig 6).

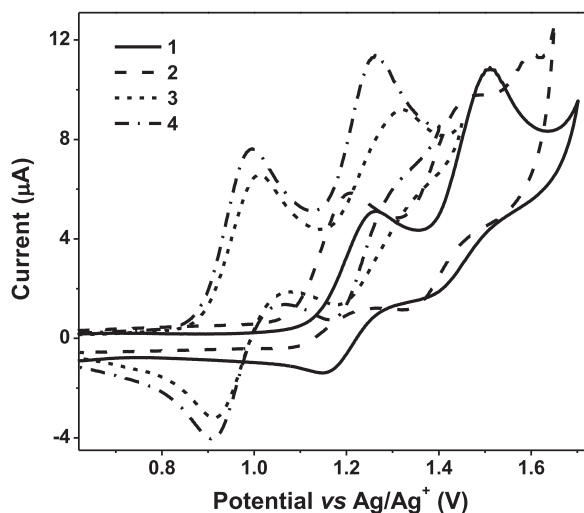


Fig. 5. CV curves of **1–4** measured in  $CH_2Cl_2$  at a scan rate of 50 mV/s.

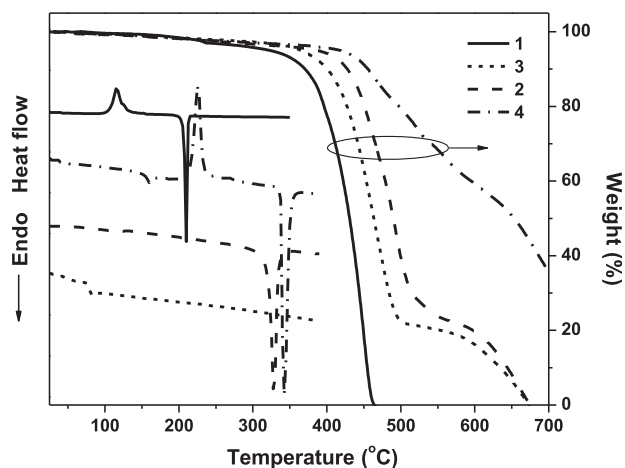


Fig. 6. DSC (second heating) and TAG thermograms of **1–4** measured under  $N_2$  at heating rate of 10 °C/min.

## 2.4. Electroluminescence properties

In order to investigate the electroluminescence properties of **1–4**, OLED devices were fabricated with the following device structure: indium tin oxide (ITO)/PEDOT:PSS/EML(50 nm)/BCP(40 nm)/LiF(0.5 nm):Al(150 nm), where these materials were used as the emitting layer (EML). Conductive polymer poly(3,4-ethylenedioxythiophene):poly(4-styrenesulfonate) (PEDOT:PSS) as hole injection layer and 2,9-dimethyl-4,7-diphenyl-1,10-phenanthroline (BCP) as hole-blocking layer were also used to enable high-performance devices. The voltage–luminance and voltage–current density ( $J$ – $V$ – $L$ ) characteristics of the devices are shown in Figs. 7 and 8, and their electrical parameters are summarized in Table 2. The results revealed that **3** and **4**, owing to the electron donating triphenylamine in the molecules had the best EML properties among these four materials. Device IV having **4** as EML showed the best performance with a high maximum brightness of 4586  $\text{cd}/\text{m}^2$  at 8.8 V, a low turn-on voltage of 4.6 V, a maximum luminous efficiency of 1.65  $\text{cd}/\text{A}$  and a maximum external quantum efficiency of 0.34%. A slightly lower device performance was observed from device III displaying maximum brightness of 2621  $\text{cd}/\text{m}^2$  at 8.6 V, turn-on voltage of 4.4 V, a maximum luminous efficiency of 1.28  $\text{cd}/\text{A}$  and a maximum external quantum efficiency of 0.26%. Devices I and II exhibited poorer device performance. The trend in device luminous efficiencies matches very well with the observed decrease in PL quantum efficiencies in going from **4** to **3** to **1** to **2** (Table 1). Fluorescence quantum yields ( $\Phi_F$ ) of both **3** and **4** were significantly higher than those of **1** and **2**. The efficiency of an OLED depends both on the balance of electrons and holes and the  $\Phi_F$  of the emitter.<sup>26</sup> Analysis of band energy diagrams of all devices also revealed that the HOMO levels of all compounds (5.32–5.56 eV) lied between those of PEDOT:PSS (5.00 eV) and BCP (6.50 eV) (see Supplementary data). However, there is a barrier around 0.32 eV for holes to migrate from the PEDOT:PSS/EML interface in devices III and IV, while such energy barrier (0.52–0.56 eV) is wider in devices I and II. This suggests that a migration of the hole from the PEDOT:PSS to EML layer is more effective in devices III and IV resulting the charge efficiently recombining in the emitting layer and better device performance. Fig. 9 showed the normalized electroluminescence (EL) spectra of all diodes. In device III and IV, the EL emission was very similar to their corresponding PL emission with emission  $\lambda_{\text{max}}$  of 457 and 465 nm, respectively. However, we observed a spectral shift in the EL spectra for compounds **1** and **2**. The EL spectrum of device I (**1** as EML) displayed an emission peak at 440 nm corresponding PL emission of compound **1** and shoulder emission owing to exciplex

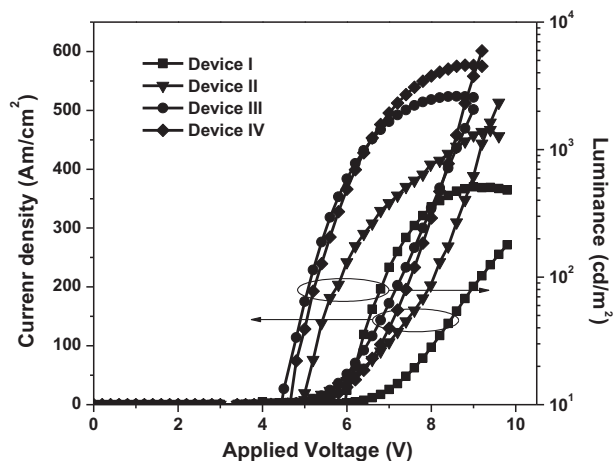


Fig. 7.  $J$ – $V$ – $L$  characteristics of OLED devices with **1–4** as EML.

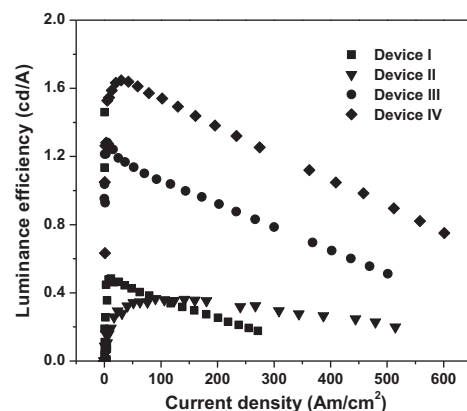


Fig. 8. Variation in luminance efficiency with current density of OLED devices with **1–4** as EML.

species at the longer wavelength, while EL spectrum of device II (**2** as EML) presented a totally red-shifted emission peak (498 nm) from the exciplex species. However, stable emission was obtained from the all diodes with the EL spectra not changing much over the entire drive voltages (see Supplementary data).

As the HOMO levels of both **3** and **4**, having a hole-transporting moiety in the molecules, matching well with the work function of ITO (4.8 eV), these compounds may potentially serve as hole-transporting materials (HTM). To test this hypothesis, double-layer green OLED devices with the structure of ITO/PEDOT:PSS/HTL(40 nm)/Alq3(50 nm)/LiF(0.5 nm):Al(150 nm) were fabricated, where these materials were used as hole-transporting layers (HTL) and tris-(8-hydroxyquinoline)aluminum (Alq3) as the green light-emitting (EML) and electron-transporting layers (ETL). The reference device with the same structure based on commonly used commercial HTM,  $N,N'$ -diphenyl- $N,N'$ -bis(1-naphthyl)-(1,1'-biphenyl)-4,4'-diamine (NPB), as HTL was made for comparison.

When comparing of HOMO and LUMO levels of layers for the devices, it was found that the HOMO levels of compounds **3** and **4** (5.32 eV) lay between those of PEDOT:PSS (5.00 eV) and Alq3 (5.80 eV), while the LUMO level of Alq3 (3.00 eV) lay between those of **3** and **4** (2.43–2.43 eV) and LiF:Al (4.20 eV) (see Supplementary data). There is a barrier of around 0.32 eV for holes to migrate from the HTL layer to Alq3 layer, while that for electron to transport from the Alq3 to the HTL layer is about 0.57 eV. According to this band diagram and device configuration, both compounds can transport a hole injected from ITO/PEDOT:PSS to the Alq3 emitting layer. Under applied voltage, all devices emitted a bright green luminescence with EL spectra ( $\lambda_{\text{max}}$  507–515 nm) matching with the PL spectrum of Alq3 and also other reported EL spectra of Alq3 devices (Fig. 10).<sup>27</sup> No emission at the longer wavelength owing to exciplex species formed at the interface of HTL and ETL materials, which is often occurred in the devices fabricated from HTL with planar molecular structure, was detected.<sup>28</sup> In our case, the formation exciplex species could be prevented by the bulky nature of both the anthracene core and triphenylamine at the peripheral of the molecules. From these results and in view of the fact that barrier for electron-migration at the Alq3/HTL interface (0.57 eV) is nearly twice higher than those for hole-migration at the HTL/Alq3 interface (0.32 eV), thus these compounds act only as HTM and Alq3 would act preferably as an electron blocker more than as a hole blocker and charge recombination thus confined to Alq3 layer.

The voltage–luminance and voltage–current density ( $J$ – $V$ – $L$ ) characteristics of the devices are shown in Figs. 11 and 12, and their electrical parameters are summarized in Table 2. These results clearly demonstrate the hole-transporting ability of **3** and **4** with superior device performance (maximum brightness and efficiency)

**Table 2**  
Device characteristics of OLEDs with **1–4** and NBP as either EML or HTL

Device	Structure	$V_{on}^a$	$\lambda_{em}^b$	$L_{max}^c$	$V_{max}^d$	$J^e$	$\eta^f$	EQE <sup>g</sup>	CIE <sup>h</sup>
I	ITO/PEDOT:PSS/ <b>1</b> /BCP/LiF:Al	5.7	440	504	9.0	237	0.48	0.10	0.15, 0.13
II	ITO/PEDOT:PSS/ <b>2</b> /BCP/LiF:Al	4.7	498	1427	9.4	479	0.37	0.03	0.22, 0.44
III	ITO/PEDOT:PSS/ <b>3</b> /BCP/LiF:Al	4.4	457	2621	8.6	436	1.28	0.26	0.14, 0.13
IV	ITO/PEDOT:PSS/ <b>4</b> /BCP/LiF:Al	4.6	465	4586	8.8	512	1.65	0.34	0.15, 0.16
V	ITO/PEDOT:PSS/ <b>3</b> /Alq3/LiF:Al	3.8	515	18,035	10.6	891	4.13	0.20	0.27, 0.52
VI	ITO/PEDOT:PSS/ <b>4</b> /Alq3/LiF:Al	4.0	509	32,270	11.4	894	6.25	0.30	0.26, 0.49
VII	ITO/PEDOT:PSS/NBP/Alq3/LiF:Al	3.4	515	30,044	11.0	1362	4.45	0.22	0.25, 0.47

<sup>a</sup> Turn-on voltage (V) at luminance of 10 cd/m<sup>2</sup>.

<sup>b</sup> Emission maximum.

<sup>c</sup> Maximum luminance (cd/m<sup>2</sup>) at the applied voltage (V).

<sup>d</sup> Voltage (V) at maximum luminance.

<sup>e</sup> Current density (mA/cm<sup>2</sup>).

<sup>f</sup> Luminance efficiency (cd/A).

<sup>g</sup> External quantum efficiency (%).

<sup>h</sup> CIE coordinates (x,y).

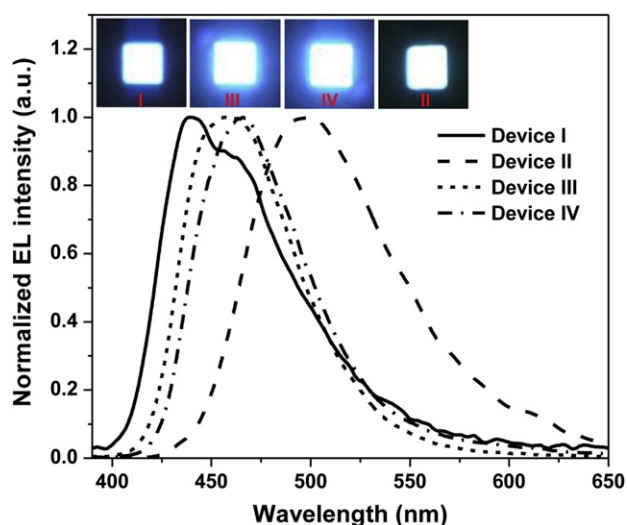


Fig. 9. EL spectra of OLED devices with **1–4** as EML.

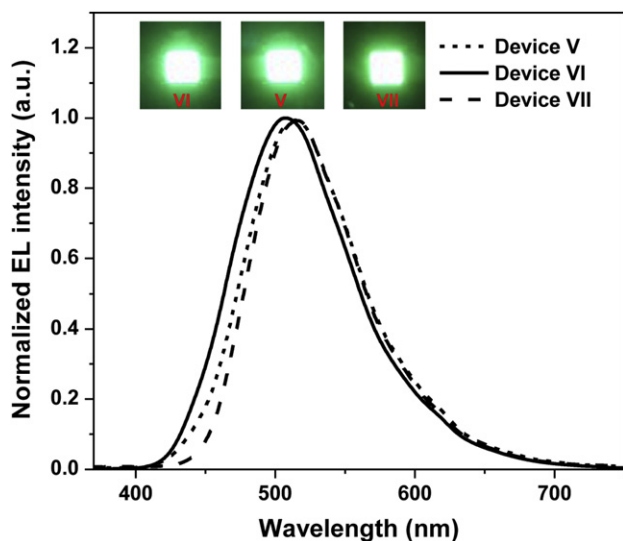


Fig. 10. EL spectra of green OLED devices with **3, 4,** and NBP as HTL.

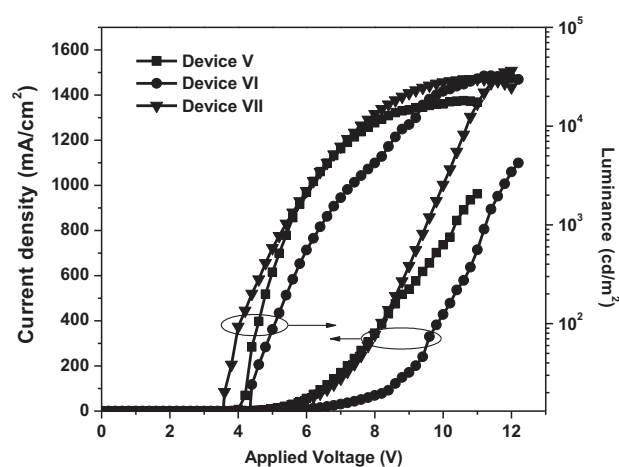


Fig. 11.  $J$ – $V$ – $L$  characteristics of green OLED devices with **3, 4,** and NBP as HTL.

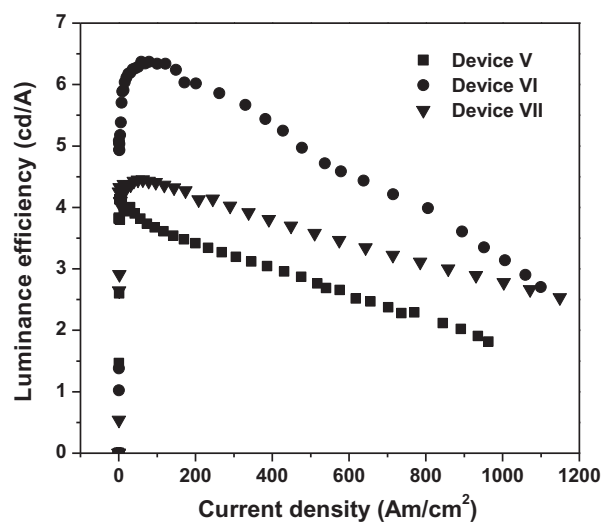


Fig. 12. Variation in luminance efficiency with current density of green OLED devices with **3, 4,** and NBP as HTL.

comparable to the NBP-based device (device VII). Device VI, having compound **4** as HTL, exhibited the best performance with a high maximum brightness of 32,270 cd/m<sup>2</sup> for green OLED at 11.4 V, a low turn-on voltage of 4 V, a maximum luminous efficiency of

6.25 cd/A and a maximum external quantum efficiency of 0.30%. A slightly lower device performance was observed from compound **3**-based device (device VI) showing a maximum brightness of 18,035 cd/m<sup>2</sup> at 10.6 V, turn-on voltage of 3.8 V, a maximum luminous efficiency of 4.13 cd/A and a maximum external quantum efficiency of 0.20%.

### 3. Conclusions

In conclusion, we have successfully synthesized four new 9,10-substituted anthracenes with the combined characteristics of light-emitting and hole-transporting materials. These materials showed blue emission with high emission quantum efficiency over 70% in the solution and strong luminance in solid state. All of them were electrochemically and thermally stable with degradation temperature well above 330 °C. Most importantly, two of these materials, having the electron donating triphenylamine as a peripheral substituent, showed promising potential as both blue light-emitting materials and hole-transporting materials for Alq3-based OLED devices. Their ability as HTL for green OLEDs was comparable to a common hole-transporter NPB. Blue OLEDs with a maximum luminance efficiency of 1.65 cd/A, and green OLEDs with maximum luminance efficiency of 6.25 cd/A were achieved.

### 4. Experimental

#### 4.1. General procedure

All reagents were purchased from Aldrich, Acros or Fluka and used without further purification. All solvents were supplied by Thai companies and used without further distillation. Tetrahydrofuran (THF) was refluxed with sodium and benzophenone, and freshly distilled prior to use. Dichloromethane for cyclic voltammetry (CV) measurements was washed with concd H<sub>2</sub>SO<sub>4</sub> and distilled twice from calcium hydride.

<sup>1</sup>H and <sup>13</sup>C nuclear magnetic resonance (NMR) spectra were recorded on a Brüker AVANCE 300 MHz spectrometer with tetramethylsilane as the internal reference using CDCl<sub>3</sub> as solvent in all cases. High resolution mass spectrometry (HRMS) was performed by Mass Spectrometry Unit at Chulabhorn Research Institute (CRI). Infrared (IR) spectra were measured on a Perkin–Elmer FTIR spectroscopy spectrum RXI spectrometer as potassium bromide (KBr) disc. Ultraviolet–visible (UV–vis) spectra were recorded as a diluted solution in spectroscopic grade dichloromethane on a Perkin–Elmer UV Lambda 25 spectrometer. Photoluminescence spectra and the fluorescence quantum yields ( $\Phi_F$ ) were recorded with a Perkin–Elmer LS 50B Luminescence Spectrometer as a dilute solution in spectroscopic grade dichloromethane and thin film obtained by thermal deposition. The fluorescence quantum yields ( $\Phi_F$ ) were determined by comparison with a fluorescence standard of known fluorescence quantum yield value according to the following equation<sup>23</sup>:

$$\Phi_x = \Phi_{ST} \left( \frac{\text{Slope}_x}{\text{Slope}_{ST}} \right) \left( \frac{\eta_x}{\eta_{ST}^2} \right) \quad (1)$$

where the subscripts *x* refer to the unknown samples and ST refers to the standard quinine sulfate solution in 0.01 M H<sub>2</sub>SO<sub>4</sub>, whose fluorescence quantum yield is known to be 0.54.  $\Phi$  is the fluorescence quantum yield, slope is the slope from the plot of integrated fluorescence intensity versus absorbance, and  $\eta$  is the refractive index of the solvent. The refractive indexes of the solvents were taken as 1.424 and 1.333 for CH<sub>2</sub>Cl<sub>2</sub> and 0.01 M H<sub>2</sub>SO<sub>4</sub>, respectively (see Supplementary data).

Differential scanning calorimetry (DSC) analysis and thermogravimetry analysis (TGA) were performed on a METTLER DSC823e thermal analyzer and a Rigaku TG-DTA 8120 thermal analyzer, respectively, with heating rate of 10 °C/min under nitrogen atmosphere. Cyclic voltammetry (CV) measurements were carried out on an Autolab Potentiostat PGSTAT 12 with a three-electrode system (platinum counter electrode, glassy carbon working electrode, and Ag/Ag<sup>+</sup> reference electrode) at scan rate of 50 mV/s in dichloromethane under argon atmosphere. The concentrations of

an analytical material and supporting electrolyte tetrabutyl ammonium hexafluorophosphate (*n*-Bu<sub>4</sub>NPF<sub>6</sub>) were 10<sup>−3</sup> M and 0.1 M, respectively. High resolution mass spectrometry (HRMS) analysis was performed by Mass Spectrometry Unit, Mahidol University, Thailand.

The ground state geometries were fully optimized using density functional theory (DFT) at the B3LYP/6-31G (d,p) level, as implemented in Gaussian 03. TDDFT/B3LYP calculation of lowest excitation energies was performed at the optimized geometries of the ground states.<sup>21</sup>

#### 4.2. Fabrication and characterization of OLEDs

OLED devices using **1–4** as EL with configuration of ITO/PEDOT:PSS/EML(50 nm)/BCP(40 nm)/LiF(0.5 nm):Al(150 nm) and double-layer green OLED devices using **3**, **4**, and NPB as HTL with configuration ITO/PEDOT:PSS/HTL(40 nm)/Alq3(50 nm)/LiF(0.5 nm):Al(150 nm) were fabricated and characterized as followed. The patterned indium tin oxide (ITO) glass substrate with a sheet resistance 14 Ω/□ (purchased from Kintec Company) was thoroughly cleaned by successive ultrasonic treatment in detergent, deionized water, isopropanol, and acetone, and then dried at 60 °C in a vacuum oven. A 50 nm thick PEDOT:PSS hole injection layer was spin-coated on top of ITO from a 0.75 wt% dispersion in water at a spin speed of 3000 rpm for 20 s and dried at 200 °C for 15 min under vacuum. Thin films of each organic EML or HTL were deposited on top of PEDOT:PSS layer by evaporation from resistively heated alumina crucibles at evaporation rate of 0.5–1.0 nm/s in vacuum evaporator deposition (ES280, ANS Technology) under a base pressure of ~10<sup>−5</sup> mbar. The film thickness was monitored and recorded by quartz oscillator thickness meter (TM-350, MAXTEK). A 40 nm thick hole-blocking layer of BCP or a 50 nm thick green-emitting layer of Alq3 was then deposited on the organic EML or HTL, respectively, without breaking the vacuum chamber. The chamber was vented with dry air to load the cathode materials and pumped back; a 0.5 nm thick LiF and a 150 nm thick aluminum layers were then subsequently deposited through a shadow mask on the top of EML/HTL film without breaking vacuum to form an active diode areas of 4 mm<sup>2</sup>. The measurement of device efficiency was performed according to M.E. Thomson's protocol and the device external quantum efficiencies were calculated using procedure reported previously.<sup>29</sup> Current density–voltage–luminescence (*J–V–L*) characteristics were measured simultaneous by the use of a Keithley 2400 source meter and a Newport 1835C power meter equipped with a Newport 818-UV/CM calibrated silicon photodiode. The EL spectra were acquired by an Ocean Optics USB4000 multichannel spectrometer. All the measurements were performed under ambient atmosphere at room temperature.

#### 4.3. Synthesis and characterization

**4.3.1. 9-Bromo-10-(9,9-dihexylfluoren-2-yl)anthracene (6).** A mixture of 2-iodo-9,9-bis-*n*-hexylfluorene (1.28 g, 2.79 mmol), 9-bromoanthracen-10-boronic acid (0.84 g, 2.79 mmol), Pd(PPh<sub>3</sub>)<sub>4</sub> (0.065 g, 0.12 mmol) and 2 M Na<sub>2</sub>CO<sub>3</sub> (8 ml) aqueous solution in THF (12 ml) was degassed with N<sub>2</sub> for 5 min. The reaction mixture was stirred at reflux under N<sub>2</sub> for 18 h. After being cooled to room temperature, water (50 ml) was added and extracted with CH<sub>2</sub>Cl<sub>2</sub> (50 ml×2). The combined organic phase was washed with water (50 ml), brine solution (50 ml), dried over anhydrous Na<sub>2</sub>SO<sub>4</sub>, filtered, and the solvents were removed to dryness. Purification by column chromatography over silica gel eluting with a mixture of CH<sub>2</sub>Cl<sub>2</sub> and hexane (1:4) followed by recrystallization from a mixture of CH<sub>2</sub>Cl<sub>2</sub> and methanol afforded the 9-bromo-10-(9,9-dihexylfluoren-2-yl) anthracene **6** (0.66 g, 52%) as a light yellow solid, mp 158 °C;  $\nu_{\text{max}}$  (KBr) 2928, 1462, 1438, 1344, 1260, 1020,

890  $\text{cm}^{-1}$ ;  $\delta_{\text{H}}$  (300 MHz,  $\text{CDCl}_3$ ) 0.76–0.88 (10H, m), 1.09–1.14 (12H, m), 1.95–2.01 (4H, m), 7.34–7.40 (7H, m), 7.59 (2H, t,  $J=8.8$  Hz), 7.72 (2H, d,  $J=9.0$  Hz), 7.81 (1H, dd,  $J=3.3, 2.7$  Hz), 7.89 (1H, d,  $J=7.5$  Hz), 8.62 (2H, d,  $J=8.7$  Hz);  $\delta_{\text{C}}$  (75 Hz,  $\text{CDCl}_3$ ) 13.99, 22.47, 23.85, 29.60, 31.52, 40.37, 55.26, 119.62, 119.83, 122.92, 124.87, 125.46, 125.91, 126.54, 126.92, 127.32, 127.44, 129.73, 130.30, 131.20, 136.90, 140.81, and 150.95; HRMS (ESI):  $[\text{MH}^+]$  found 589.3042.  $\text{C}_{39}\text{H}_{42}\text{Br}$  requires 589.2432.

**4.3.2. 9-(9,9-Dihexylfluoren-2-yl)-10-thiophen-2-yl-anthracene (1).** A mixture of **6** (0.67 g, 1.14 mmol), 2-thiopheneboronic acid (0.16 g, 1.25 mmol),  $\text{Pd}(\text{PPh}_3)_4$  (0.025 g, 0.023 mmol), and 2 M  $\text{Na}_2\text{CO}_3$  aqueous solution (6 ml) in THF (10 ml) was degassed with  $\text{N}_2$  for 5 min. The reaction mixture was stirred at reflux under  $\text{N}_2$  for 20 h. After being cooled to room temperature, water (50 ml) was added and extracted with  $\text{CH}_2\text{Cl}_2$  (50 ml $\times$ 2). The combined organic phase was washed with water (50 ml), brine solution (50 ml), dried over anhydrous  $\text{Na}_2\text{SO}_4$ , filtered, and the solvents were removed to dryness. Purification by column chromatography over silica gel eluting with a mixture of  $\text{CH}_2\text{Cl}_2$  and hexane (1:4) followed by recrystallization from a mixture of  $\text{CH}_2\text{Cl}_2$  and methanol afforded the 9-(9,9-dihexylfluoren-2-yl)-10-thiophen-2-yl-anthracene **1** (0.51 g, 76%) as a light yellow solid, mp 186 °C;  $\nu_{\text{max}}$  (KBr) 2930, 1458, 1440, 1380, 1224, 1028, 824  $\text{cm}^{-1}$ ;  $\delta_{\text{H}}$  (300 MHz,  $\text{CDCl}_3$ ) 0.78–0.82 (10H, m), 1.12–1.18 (12H, m), 2.03 (4H, t,  $J=9.0$  Hz), 7.34–7.47 (11H, m), 7.66 (1H, d,  $J=4.8$  Hz), 7.79 (2H, d,  $J=8.7$  Hz), 7.84 (1H, d,  $J=7.8$  Hz), 7.92–7.98 (3H, m);  $\delta_{\text{C}}$  (75 Hz,  $\text{CDCl}_3$ ) 14.03, 22.51, 23.89, 29.66, 31.55, 40.45, 55.27, 119.64, 119.82, 122.92, 125.10, 125.57, 126.03, 126.73, 126.91, 127.03, 127.20, 127.26, 128.66, 129.50, 129.75, 131.65, 137.40, 139.17, 139.31, 140.87, 141.05, 150.91, 151.02; HRMS (ESI):  $[\text{MH}^+]$  found 593.3186.  $\text{C}_{43}\text{H}_{45}\text{S}$  requires 593.3197.

**4.3.3. 2-Bromo-5-(10-(9,9-dihexylfluoren-2-yl)anthracen-9-yl)thiophene (7).** To a solution of **1** (0.60 g, 1.01 mmol) in tetrahydrofuran (15 ml) was added NBS (0.18 g, 1.01 mmol) in small portions. While adding NBS, the reaction was monitored by TLC. Soon after the starting material was consumed, water was added and the mixture was extracted with  $\text{CH}_2\text{Cl}_2$  (50 ml $\times$ 2). The combined organic phase was washed with water (50 ml), a dilute  $\text{NaHCO}_3$  aqueous solution (50 ml), brine solution (50 ml), dried over anhydrous  $\text{Na}_2\text{SO}_4$ , filtered, and the solvents were removed to dryness. Purification by recrystallization of a mixture of  $\text{CH}_2\text{Cl}_2$  and methanol gave the 2-bromo-5-(10-(9,9-dihexylfluoren-2-yl)anthracen-9-yl)thiophene **7** (0.64 g, 95%) as a light yellow solid, mp 191 °C;  $\nu_{\text{max}}$  (KBr) 2926, 1469, 1433, 1334, 1261, 1020, 878  $\text{cm}^{-1}$ ;  $\delta_{\text{H}}$  (300 MHz,  $\text{CDCl}_3$ ) 0.74–0.92 (10H, m), 1.08–1.15 (12H, m), 1.97–2.05 (4H, m), 6.99 (1H, d,  $J=3.9$  Hz), 7.29–7.47 (10H, m), 7.75 (2H, d,  $J=8.7$  Hz), 7.81–7.84 (1H, m), and 7.92–7.97 (3H, m);  $\delta_{\text{C}}$  (75 Hz,  $\text{CDCl}_3$ ) 14.00, 22.49, 23.87, 29.63, 31.53, 40.42, 55.26, 112.83, 119.65, 119.82, 122.92, 125.17, 125.91, 126.37, 126.91, 127.13, 127.30, 128.87, 129.67, 129.94, 130.14, 131.56, 134.10, 137.16, 139.81, 140.76, 140.87, 141.18, 150.91, 150.96; HRMS (ESI):  $[\text{MH}^+]$  found 671.5429.  $\text{C}_{43}\text{H}_{44}\text{BrS}$  requires 671.2349.

**4.3.4. 5,5'-Bis(10-(9,9-dihexylfluoren-2-yl)anthracen-9-yl)-2,2'-bithiophene (2).** A mixture of **7** (0.65 g, 0.96 mmol),  $\text{NiCl}_2$  (0.75 g, 5.78 mmol), Zn powder (0.11 g, 1.73 mmol),  $\text{PPh}_3$  (0.15 g, 0.57 mmol), and bipyridine (bpy) (0.06 g, 0.38 mmol) in DMAc (10 ml) was degassed with  $\text{N}_2$  for 10 min. The reaction mixture was stirred at reflux under  $\text{N}_2$  for 24 h. After being cooled to room temperature, water (50 ml) was added and extracted with  $\text{CH}_2\text{Cl}_2$  (50 ml $\times$ 2). The combined organic phase was washed with water (50 ml), brine solution (50 ml), dried over anhydrous  $\text{Na}_2\text{SO}_4$ , filtered, and the solvents were removed to dryness. Purification by column chromatography over silica gel eluting with a mixture of  $\text{CH}_2\text{Cl}_2$  and hexane (1:5) followed by recrystallization from a mixture of  $\text{CH}_2\text{Cl}_2$  and methanol afforded the 5,5'-bis(10-(9,9-dihexylfluoren-2-yl)

anthracen-9-yl)-2,2'-bithiophene **2** (0.35 g, 63%) as a greenish solid, mp >250 °C;  $\nu_{\text{max}}$  (KBr) 2922, 1557, 1447, 1369, 1270, 1018, 824, 764  $\text{cm}^{-1}$ ;  $\delta_{\text{H}}$  (300 MHz,  $\text{CDCl}_3$ ) 0.78–0.82 (20H, m), 1.12–1.18 (24H, m), 2.03 (8H, t,  $J=8.1$  Hz), 7.22 (2H, d,  $J=3.3$  Hz), 7.36–7.55 (20H, m), 7.80–7.87 (6H, m), 7.95 (2H, d,  $J=8.1$  Hz), 8.12 (4H, d,  $J=9.0$  Hz);  $\delta_{\text{C}}$  (75 Hz,  $\text{CDCl}_3$ ) 14.01, 22.50, 23.89, 29.65, 31.54, 40.44, 55.28, 119.65, 119.82, 122.93, 123.88, 125.18, 125.78, 126.02, 126.69, 127.13, 127.27, 128.04, 129.75, 130.04, 130.49, 131.60, 137.33, 138.50, 138.73, 139.48, 140.73, 140.92, 150.91, 150.99; HRMS (ESI):  $[\text{MH}^+]$  found 1183.6210.  $\text{C}_{86}\text{H}_{87}\text{S}_2$  requires 1183.6244.

**4.3.5. 9-(9,9-Dihexylfluoren-2-yl)-10-(4-diphenylaminophenyl)anthracene (3).** A mixture of **6** (0.52 g, 0.88 mmol), *N,N*-diphenyl-*N*-4-aminophenylboronic acid (0.28 g, 0.97 mmol),  $\text{Pd}(\text{PPh}_3)_4$  (0.021 g, 0.017 mmol), and 2 M  $\text{Na}_2\text{CO}_3$  aqueous solution (6 ml) in THF (10 ml) was degassed with  $\text{N}_2$  for 5 min. The reaction mixture was stirred at reflux under  $\text{N}_2$ . After being cooled to room temperature, water (50 ml) was added and extracted with  $\text{CH}_2\text{Cl}_2$  (50 ml $\times$ 2). The combined organic phase was washed with water (50 ml), brine solution (50 ml), dried over anhydrous  $\text{Na}_2\text{SO}_4$ , filtered, and the solvents were removed to dryness. Purification by column chromatography over silica gel eluting with a mixture of  $\text{CH}_2\text{Cl}_2$  and hexane (1:4) followed by recrystallization from a mixture of  $\text{CH}_2\text{Cl}_2$  and methanol afforded the 9-(9,9-dihexylfluoren-2-yl)-10-(4-diphenylaminophenyl) anthracene **3** (0.52 g, 79%) as a light yellow solid, mp 146 °C;  $\nu_{\text{max}}$  (KBr) 2929, 1590, 1494, 1380, 1273, 1019, 823, 746  $\text{cm}^{-1}$ ;  $\delta_{\text{H}}$  (300 MHz,  $\text{CDCl}_3$ ) 0.75–0.80 (10H, m), 1.09–1.16 (12H, m), 1.98–2.03 (4H, m), 7.07–7.12 (2H, t,  $J=7.0$  Hz), 7.26–7.46 (21H, m), 7.77–7.95 (6H, m);  $\delta_{\text{C}}$  (75 Hz,  $\text{CDCl}_3$ ) 14.02, 22.51, 23.89, 31.55, 40.47, 55.26, 119.61, 119.78, 122.91, 123.10, 123.13, 124.71, 124.97, 126.16, 126.88, 127.10, 127.19, 129.40, 129.89, 130.10, 130.15, 132.14, 132.69, 136.92, 137.70, 140.54, 141.00, 147.17, 147.84, 150.86, 150.98; HRMS (ESI):  $[\text{MH}^+]$  found 754.4386.  $\text{C}_{57}\text{H}_{56}\text{N}$  requires 754.4407.

**4.3.6. 2,7-Bis(9-bromoanthracene-10-yl)-9,9-dihexylfluorene (9).** A mixture of 2,7-diiodo-9,9-bis-*n*-hexylfluorene (1.11 g, 1.90 mmol), 9-bromoanthracen-10-boronic acid (1.20 g, 3.99 mmol),  $\text{Pd}(\text{PPh}_3)_4$  (0.11 g, 0.10 mmol), and 2 M  $\text{Na}_2\text{CO}_3$  (10 ml) aqueous solution in THF (15 ml) was degassed with  $\text{N}_2$  for 5 min. The reaction mixture was stirred at reflux under  $\text{N}_2$  for 20 h. After being cooled to room temperature, water (50 ml) was added and extracted with  $\text{CH}_2\text{Cl}_2$  (50 ml $\times$ 2). The combined organic phase was washed with water (50 ml), brine solution (50 ml), dried over anhydrous  $\text{Na}_2\text{SO}_4$ , filtered, and the solvents were removed to dryness. Purification by column chromatography over silica gel eluting with a mixture of  $\text{CH}_2\text{Cl}_2$  and hexane (1:4) followed by recrystallization from a mixture of  $\text{CH}_2\text{Cl}_2$  and methanol afforded the 2,7-bis(9-bromoanthracene-10-yl)-9,9-dihexylfluorene **9** (0.90 g, 56%) as a light yellow solid, mp 188 °C;  $\nu_{\text{max}}$  (KBr) 2927, 1460, 1440, 1340, 1261, 1020, 893  $\text{cm}^{-1}$ ;  $\delta_{\text{H}}$  (300 MHz,  $\text{CDCl}_3$ ) 0.8 (6H, t,  $J=6.9$  Hz), 0.94 (4H, m), 1.14–1.27 (12H, m), 2.04 (4H, t,  $J=7.8$  Hz), 7.40–7.48 (8H, m), 7.65 (4H, t,  $J=8.4$  Hz), 7.79 (4H, d,  $J=9.0$  Hz), 8.04 (2H, d,  $J=8.1$  Hz), 8.66 (4H, d,  $J=9.0$  Hz);  $\delta_{\text{C}}$  (75 Hz,  $\text{CDCl}_3$ ) 14.02, 22.40, 24.06, 29.55, 31.57, 40.34, 55.51, 119.86, 122.70, 125.56, 126.04, 126.97, 127.40, 127.95, 130.01, 130.34, 131.21, 137.32, 138.229, 140.53, 151.21; HRMS (ESI):  $[\text{MH}^+]$  found 843.8920.  $\text{C}_{53}\text{H}_{49}\text{Br}_2$  requires 843.2193.

**4.3.7. 2,7-Bis(9-(4-diphenylaminophenyl)anthracene-10-yl)-9,9-dihexylfluorene (4).** A mixture of **9** (0.51 g, 0.60 mmol), *N,N*-diphenyl-*N*-4-aminophenylboronic acid (0.37 g, 1.27 mmol),  $\text{Pd}(\text{PPh}_3)_4$  (0.01 g, 0.01 mmol), and 2 M  $\text{Na}_2\text{CO}_3$  aqueous solution (6 ml) in THF (10 ml) was degassed with  $\text{N}_2$  for 5 min. The reaction mixture was stirred at reflux under  $\text{N}_2$ . After being cooled to room temperature, water (50 ml) was added and extracted with  $\text{CH}_2\text{Cl}_2$  (50 ml $\times$ 2). The combined organic phase was washed with water (50 ml), brine solution (50 ml), dried over anhydrous  $\text{Na}_2\text{SO}_4$ , filtered,

and the solvents were removed to dryness. Purification by column chromatography over silica gel eluting with a mixture of  $\text{CH}_2\text{Cl}_2$  and hexane (1:6) followed by recrystallization from a mixture of  $\text{CH}_2\text{Cl}_2$  and methanol afforded the 2,7-bis(9-(4-diphenylaminophenyl)anthracene-10-yl)-9,9-dihexylfluorene **4** (0.45 g, 75%) as a deep yellow solid, mp  $>250^\circ\text{C}$ ;  $\nu_{\text{max}}$  (KBr) 2922, 1590, 1491, 1384, 1273, 1019, 823, 764  $\text{cm}^{-1}$ ;  $\delta_{\text{H}}$  (300 MHz,  $\text{CDCl}_3$ ) 0.82 (6H, t,  $J=6.9$  Hz), 0.91 (4H, br s), 1.17–1.28 (12H, m), 2.06 (4H, t,  $J=7.8$  Hz), 7.12 (4H, t,  $J=6.9$  Hz), 7.31–7.48 (32H, m), 7.55–7.56 (4H, m), 7.85 (4H, d,  $J=8.7$  Hz), 7.90 (4H, d,  $J=8.4$  Hz), 8.07 (2H, d,  $J=8.1$  Hz);  $\delta_{\text{C}}$  (75 Hz,  $\text{CDCl}_3$ ) 14.05, 22.48, 24.10, 29.65, 31.62, 40.51, 55.50, 119.77, 123.12, 124.73, 125.02, 126.28, 127.07, 127.16, 129.41, 130.14, 130.20, 132.16, 132.70, 137.00, 137.55, 137.96, 140.43, 147.20, 147.85, 151.18; HRMS (ESI):  $[\text{M}]^+$  found 1173.6070.  $\text{C}_{89}\text{H}_{77}\text{N}_2$  requires 1173.6081.

## Acknowledgements

This work was financially supported by the Thailand Research Fund (RMU5080052). We acknowledge the scholarship support from Center of Excellence for Innovation in Chemistry (PERCH-CIC), Ubon Ratchathani University, and the Strategic Scholarships for Frontier Research Network for Research Groups (CHE-RES-RG50) from the Office of the Higher Education Commission, Thailand.

## Supplementary data

$^1\text{H}$  NMR and  $^{13}\text{C}$  NMR spectra, and more results for theoretical calculation, quantum yield, CV curve, band energy diagram of OLED devices, and EL spectra. Supplementary data related to this article can be found online at doi:10.1016/j.tet.2011.12.083.

## References and notes

- Tang, C. W.; van Slyke, S. A. *Appl. Phys. Lett.* **1987**, *51*, 913–915.
- (a) Brunner, K.; Van Dijken, A.; Börner, H.; Bastiaansen, J. J. A. M.; Kiggen, N. M. M.; Langeveld, B. M. W. *J. Am. Chem. Soc.* **2004**, *126*, 6035–6042; (b) Kim, Y. H.; Lee, S. J.; Byeon, K. N.; Kim, J. S.; Shin, S. C.; Kwon, S. K. *Bull. Korean Chem. Soc.* **2007**, *28*, 443–444.
- (a) Wong, K.-T.; Chien, Y.-Y.; Chen, R.-T.; Wang, C.-F.; Lin, Y.-T.; Chiang, H.-H.; Hsieh, P.-Y.; Wu, C.-C.; Chou, C. H.; Su, Y. O.; Lee, G. H.; Peng, S.-M. *J. Am. Chem. Soc.* **2002**, *124*, 11576–11577; (b) Jia, W.-L.; McCormick, T.; Liu, Q.-D.; Fukutani, H.; Motala, M.; Wang, R.-Y.; Tao, Y.; Wang, S. J. *Mater. Chem.* **2004**, *14*, 3344–3350.
- (a) Wu, C.-H.; Chien, C.-H.; Hsu, F.-M.; Shih, P.-I.; Shu, C.-F. *J. Mater. Chem.* **2009**, *19*, 1464–1470; (b) Kim, Y.-H.; Jeong, H.-C.; Kim, S.-H.; Yang, K.; Kwon, S.-K. *Adv. Funct. Mater.* **2005**, *15*, 1799–1805.
- (a) Crawford, G. P. *Flexible Flat Panel Displays*; John Wiley & Sons: London, 2005; 285–312; (b) Visser, P. *Optik Photonik* **2008**, *3*, 27–29; (c) Halford, E. *Chem. Eng. News* **2004**, *82*, 13.
- (a) Tao, S.; Zhou, Y.; Lee, C.-S.; Lee, S.-T.; Huang, D.; Zhang, X. *J. Phys. Chem. C* **2008**, *112*, 14603–14606; (b) Wang, J.; Wan, W.; Jiang, H.; Gao, Y.; Jiang, X.; Lin, H.; Zhao, W.; Hao, J. *Org. Lett.* **2010**, *12*, 3874–3877; (c) Shen, W.-J.; Dodda, R.; Wu, C.-C.; Wu, F.-I.; Liu, T.-H.; Chen, H.-H.; Chen, C. H.; Shu, C.-F. *Chem. Mater.* **2004**, *16*, 930–934; (d) Zhang, G.; Yang, G.; Wang, S.; Chen, Q.; Ma, J. S. *Chem.—Eur. J.* **2007**, *13*, 3630–3635; (e) Shih, P.-I.; Chuang, C.-Y.; Chien, C.-H.; Diau, E. W.-G.; Shu, C.-F. *Adv. Funct. Mater.* **2007**, *17*, 3141–3146; (f) Wee, K.-R.; Han, W.-S.; Kim, J.-E.; Kim, A.-L.; Kwon, S.; Kang, S. O. *J. Mater. Chem.* **2011**, *21*, 1115–1123; (g) Park, J. W.; Kim, Y. H.; Jung, S. Y.; Byeon, K. N.; Jang, S. H.; Lee, S. K. *Thin Solid Films* **2008**, *516*, 8381–8385.
- (a) Kim, J.-H.; Noh, S.; Kim, K.; Lim, S.-T.; Shin, D.-M. *Synth. Met.* **2001**, *117*, 227–228; (b) Kim, J.-U.; Lee, H.-B.; Shin, J.-S.; Kim, Y.-H.; Joe, Y.-K.; Oh, H.-Y.; Park, C.-G.; Kwon, S.-K. *Synth. Met.* **2005**, *150*, 27–32; (c) Yang, Z.; Chi, Z.; Yu, T.; Zhang, X.; Chen, M.; Xu, B.; Liu, S.; Zhang, Y.; Xu, J. *J. Mater. Chem.* **2009**, *19*, 5541–5546; (d) Hosokawa, C.; Higashi, H.; Nakamura, H.; Kusumoto, T. *Appl. Phys. Lett.* **1995**, *67*, 3853–3856; (e) Wong, K.-T.; Hung, T. S.; Lin, Y.; Wu, C.-C.; Lee, G.-H.; Peng, S.-M.; Chou, C. H.; Su, Y. O. *Org. Lett.* **2002**, *4*, 513–516.
- (a) Kumchoo, T.; Promarak, V.; Sudyoadsuk, T.; Sukwattanasinnit, M.; Rathsasakhon, P. *Chem. Asian J.* **2010**, *5*, 2162–2167; (b) Wu, K.-C.; Ku, P.-J.; Lin, C.-S.; Shih, H.-T.; Wu, F.-I.; Huang, M.-J.; Lin, J.-J.; Chen, I.-C.; Cheng, C.-H. *Adv. Funct. Mater.* **2008**, *18*, 67–75; (c) Kawano, S.-I.; Yang, C.; Ribas, M.; Balushev, S.; Baumgarten, M.; Mullen, K. *Macromolecules* **2008**, *41*, 7933–7937; (d) Oh, H.-Y.; Lee, C.; Lee, S. *Org. Electron.* **2009**, *10*, 163–169.
- (a) Chao, T. C.; Lin, Y. T.; Yang, C. Y.; Hung, T. S.; Chou, H. C.; Wu, C. C. *Adv. Mater.* **2005**, *17*, 992–995; (b) Gather, M. C.; Heeney, M.; Zhang, W.; Whitehead, K. S.; Bradley, D. D. C.; McCulloch, I.; Campbell, A. J. *Chem. Commun.* **2008**, 1079–1081; (c) Wu, F.-I.; Dodda, R.; Reddy, D. S.; Shu, C.-F. *J. Mater. Chem.* **2002**, *12*, 2893–2897; (d) Goel, A.; Chaurasia, S.; Dixit, M.; Kumar, V.; Prakash, S.; Jena, B.; Verma, J. K.; Jain, M.; Anand, R. S.; Manoharan, S. S. *Org. Lett.* **2009**, *11*, 1289–1292; (e) Jeon, Y.-M.; Kim, J.-W.; Lee, C.-W.; Gong, M.-S. *Dyes Pigments* **2009**, *83*, 66–71; (f) Kim, K.-S.; Jeon, Y.-M.; Kim, J.-W.; Lee, C.-W.; Gong, M.-S. *Org. Electron.* **2008**, *9*, 797–804; (g) Zhao, Z.; Xu, X.; Chen, X.; Wang, X.; Lu, P.; Yu, G.; Liu, Y. *Tetrahedron* **2008**, *64*, 2658–2668; (h) Fischer, A. L.; Linton, K. E.; Kamtekar, K. T.; Pearson, C.; Bryce, M. R.; Petty, M. C. *Chem. Mater.* **2011**, *23*, 1640–1642.
- (a) Romero, D. B.; Schaer, M.; Leclerc, M.; Adès, D.; Siove, A.; Zuppiroli, L. *Synth. Met.* **1996**, *80*, 271–277; (b) Yang, Z.; Chi, Z.; Zhou, L.; Zhang, X.; Chen, M.; Xu, B.; Wang, C.; Zhang, Y.; Xu, J. *Opt. Mater.* **2009**, *32*, 398–401; (c) Agarwal, N.; Nayak, P. K.; Ali, F.; Patankar, M. P.; Narasimhan, K. L.; Periasamy, N. *Synth. Met.* **2011**, *161*, 466–473; (d) Mori, T.; Shinnai, T.; Kijima, M. *Polym. Chem.* **2011**, *2*, 2830–2834.
- (a) Lai, S.-L.; Tong, Q.-X.; Chan, M.-Y.; Ng, T.-W.; Lo, M.-F.; Lee, S.-T.; Lee, C.-S. *J. Mater. Chem.* **2011**, *21*, 1206–1211; (b) Fang, Q.; Xu, B.; Jiang, B.; Fu, H.; Zhu, W.; Jiang, X.; Zhang, Z. *Synth. Met.* **2005**, *155*, 206–210; (c) Park, J.-W.; Kang, P.; Park, H.; Oh, H.-Y.; Yang, J.-H.; Kim, Y.-H.; Kwon, S.-K. *Dyes Pigments* **2010**, *85*, 93–98; (d) Li, Z. H.; Wong, M. S.; Tao, Y.; Lu, J. *Chem.—Eur. J.* **2005**, *11*, 3285–3293.
- (a) Sajoto, T.; Djurovich, P. I.; Tamayo, A. B.; Oxgaard, J.; Goddar, W. A., III; Thompson, M. E. *J. Am. Chem. Soc.* **2009**, *131*, 9813–9822; (b) He, L.; Duan, L.; Qiao, J.; Wang, R.; Wei, P.; Wang, L.; Qiu, Y. *Adv. Funct. Mater.* **2008**, *18*, 2123–2131; (c) Ragni, R.; Plummer, E. A.; Brunner, K.; Hofstraat, J. W.; Abudri, F.; Farinola, G. M.; Naso, F.; De Cola, L. *J. Mater. Chem.* **2006**, *16*, 1161–1170; (d) Seo, H.-J.; Yoo, K.-M.; Song, M.; Park, J. S.; Jin, S.-H.; Kim, Y. I.; Kim, J.-J. *Org. Electron.* **2010**, *11*, 564–572; (e) Seo, J. H.; Kim, Y. K.; Ha, Y. *Thin Solid Films* **2009**, *517*, 1807–1810.
- (a) Caballero, A.; Tormos, R.; Espinosa, A.; Velasco, M. D.; Tarraga, A.; Miranda, M. A.; Molina, P. *Org. Lett.* **2004**, *6*, 4599–4602; (b) Bolletta, F.; Garelli, A.; Montalti, M.; Prodi, L.; Romano, S.; Zaccheroni, N.; Canovese, L.; Chessa, G.; Santo, C.; Visentin, F. *Inorg. Chim. Acta* **2004**, *357*, 4078–4084; (c) Miyajii, H.; Anzenbacher, P., Jr.; Sessler, J. L.; Bleasdale, E. R.; Gale, P. A. *Chem. Commun.* **1999**, 1723–1724; (d) Kaur, G.; Fang, H.; Gao, X.; Li, H.; Wang, B. *Tetrahedron* **2006**, *62*, 1–8.
- (a) Mikroyannidis, J. A. *Polymer* **2000**, *41*, 8193–8204; (b) Klärner, G.; Davey, M. H.; Chen, W. D.; Scott, J. C.; Miller, R. D. *Adv. Mater.* **1998**, *10*, 993–997; (c) Chocho, S. L.; Govaris, G. K.; Kakali, F.; Yiannoulis, P.; Kallitsis, J. K. *Polymer* **2005**, *46*, 4654–4663; (d) Lee, J.-I.; Hwang, D.-H.; Park, H.; Do, L.-M.; Chu, H. Y.; Zyung, T.; Miller, R. D. *Synth. Met.* **2000**, *111–112*, 195–197.
- Boyd, T. J.; Geerts, Y.; Lee, J.-K.; Fogg, D. E.; Lavoie, G. G.; Schrock, R. R.; Rubner, M. F. *Macromolecules* **1997**, *30*, 3553–3559.
- (a) Gebeyehu, D.; Walzer, K.; He, G.; Pfeiffer, M.; Leo, K.; Brandt, J.; Gerhard, A.; Stöbel, P.; Vestweber, H. *Synth. Met.* **2005**, *148*, 205–211; (b) Zhang, Z. L.; Jiang, X. Y.; Zhu, W. Q.; Zheng, X. Y.; Wu, Y. Z.; Xu, S. H. *Synth. Met.* **2000**, *137*, 1141–1142; (c) Cha, S. W.; Choi, S.-H.; Kim, K.; Jin, J.-I. *J. Mater. Chem.* **2003**, *13*, 1900–1904.
- (a) Promarak, V.; Pankvung, A.; Jungstittiwong, S.; Saengsuwan, S.; Sudyoadsuk, T.; Keawin, T. *Tetrahedron Lett.* **2007**, *48*, 3661–3665; (b) Promarak, V.; Pankvung, A.; Ruchirawat, S. *Tetrahedron Lett.* **2007**, *48*, 1151–1154.
- (a) Gao, Z. Q.; Li, Z. H.; Xia, P. F.; Wong, M. S.; Cheah, K. W.; Chen, C. H. *Adv. Funct. Mater.* **2007**, *17*, 3194–3199; (b) Xia, H.; He, J.; Xu, B.; Wen, S.; Li, Y.; Tian, W. *Tetrahedron* **2008**, *64*, 5736–5742.
- Kelley, C. J.; Ghiorghis, A.; Kauffman, J. M. *J. Chem. Res., Minireprint* **1997**, 2701–2709.
- Promarak, V.; Ichikawa, M.; Sudyoadsuk, T.; Saengsuwan, S.; Keawin, T. *Opt. Mater.* **2007**, *30*, 364–369.
- Frisch, M. J.; Trucks, G. W.; Schlegel, H. B.; Scuseria, G. E.; Robb, M. A.; Cheeseman, J. R.; Zakrzewski, V. G.; Montgomery, J. A., Jr.; Stratmann, R. E.; Burant, J. C.; Dapprich, S.; Millam, J. M.; Daniels, A. D.; Kudin, K. N.; Strain, M. C.; Farkas, O.; Tomasi, J.; Barone, V.; Cossi, M.; Cammi, R.; Mennucci, B.; Pomelli, C.; Adamo, C.; Clifford, S.; Ochterski, J.; Petersson, G. A.; Ayala, P. Y.; Cui, Q.; Morokuma, K.; Malick, D. K.; Rabuck, A. D.; Raghavachari, K.; Foresman, J. B.; Cioslowski, J.; Ortiz, J. V.; Stefanov, B. B.; Liu, G.; Liashenko, A.; Piskorz, P.; Komaromi, I.; Gomperts, R.; Martin, R. L.; Fox, D. J.; Keith, T.; Al-Laham, M. A.; Peng, C. Y.; Nanayakkara, A.; Gonzalez, C.; Challacombe, M.; Gill, P. M. W.; Johnson, B. G.; Chen, W.; Wong, M. W.; Andres, J. L.; Head-Gordon, M.; Replogle, E. S.; Pople, J. A. *Gaussian 98, Revision A.7*; Gaussian: Pittsburgh, PA, 1998.
- Wong, K.-T.; Wang, C.-F.; Chou, C. H.; Su, Y. O.; Lee, G.-H.; Peng, S.-M. *Org. Lett.* **2002**, *4*, 4439–4442.
- Kartens, T.; Kobs, K. J. *Phys. Chem.* **1980**, *84*, 1871–1882.
- Kamtekar, K. T.; Wang, C.; Bettington, S.; Batsanov, A. S.; Perepichka, I. F.; Bryce, M. R.; Ahn, J. H.; Rabinal, M.; Petty, M. C. *J. Mater. Chem.* **2006**, *16*, 3823–3835.
- Promarak, V.; Pankvung, A.; Meunmat, D.; Sudyoadsuk, T.; Saengsuwan, S.; Keawin, T. *Tetrahedron Lett.* **2007**, *48*, 919–923.
- Mitschke, U.; BaEuerle, P. *J. Mater. Chem.* **2000**, *10*, 1471–1507.
- (a) Giro, G.; Cocchi, M.; Kalinowski, J.; Fattori, V.; Marco, P. D.; Dembech, P.; Seconi, G. *Adv. Mater. Opt. Electron.* **1999**, *9*, 189–194; (b) Tong, Q.-X.; Lai, S.-L.; Chan, M.-Y.; Lai, K.-H.; Tang, J.-X.; Kwong, H.-L.; Lee, C.-S.; Lee, S.-T. *Chem. Mater.* **2007**, *19*, 5851–5855; (c) Kim, Y. K.; Hwang, S.-H. *Synth. Met.* **2006**, *156*, 1028–1035.
- Promarak, V.; Ichikawa, M.; Sudyoadsuk, T.; Saengsuwan, S.; Jungstittiwong, S.; Keawin, T. *Synth. Met.* **2007**, *157*, 17–22.
- Forrest, S. R.; Bradley, D. D. C.; Thomson, M. E. *Adv. Mater.* **2003**, *15*, 1043–1048.